MATERIALS SCIENCE

Chemically tuned intermediate band states in atomically thin Cu$_x$GeSe/SnS quantum material for photovoltaic applications

Srihari M. Kastuar and Chinedu E. Ekuma*

A new generation of quantum material derived from intercalating zerovalent atoms such as Cu into the intrinsic van der Waals gap at the interface of atomically thin two-dimensional GeSe/SnS heterostructure is designed, and their optoelectronic features are explored for next-generation photovoltaic applications. Advanced ab initio modeling reveals that many-body effects induce intermediate band (IB) states, with subband gaps (~0.78 and 1.26 electron volts) ideal for next-generation solar devices, which promise efficiency greater than the Shockley-Queisser limit of ~32%. The charge carriers across the heterojunction are both energetically and spontaneously spatially confined, reducing nonradiative recombination and boosting quantum efficiency. Using this IB material in a solar cell prototype enhances absorption and carrier generation in the near-infrared to visible light range. Tuning the active layer's thickness increases optical activity at wavelengths greater than 600 nm, achieving ~190% external quantum efficiency over a broad solar wavelength range, underscoring its potential in advanced photovoltaic technology.

INTRODUCTION

The need for sustainable and clean energy sources has never been greater, and solar energy has emerged as a promising solution. To meet the growing demand for efficient and cost-effective solar cells, researchers are constantly exploring emerging and innovative approaches to enhance the performance of solar cells. One exciting development in this field is the concept of intermediate band solar cells (IBSCs), an emerging technology that has the potential to revolutionize clean energy generation by enabling the efficient conversion of sunlight into electrical energy beyond the Shockley-Queisser limit [~32% for single-gap solar cells (SGSCs) (1)] to efficiency as high as ~63% (2). In a typical intermediate band system, solar radiation can excite carriers from the valence to the conduction band through two pathways: direct excitation from the valence band to the conduction band, or a stepwise excitation from the valence band to the intermediate band and then to the conduction band. To efficiently capture solar energy, it is essential to engineer the material carefully and match these three transitions to the solar radiation. This enables a single photon to result in multiple exciton generations (MEG) through a two-step absorption process, even for photons with energies slightly above the bandgap. This is unlike SGSCs where MEG only occurs when the solar photon energy is at least twice the bandgap (3, 4).

At the forefront of the search for advanced materials for IBSC application is nanoscale systems such as self-assembled quantum dots and impurity-doped semiconductors (5, 6). However, the realization of intermediate band materials has been hindered by the lack of suitable materials with the desirable properties at ambient conditions. Midgap states, which can be engineered through impurity and defect states, can markedly increase the efficiency of solar cells, but only if the midgap (intermediate) states are doped beyond the Mott-Anderson transition (7), which is challenging because of the solubility limit (8). Unlike in impurity photovoltaics, the midgap states for IBSC application must be isolated from both the conduction band and valence band to avoid electron-phonon interaction that can produce thermal relaxations. Moreover, the intermediate band must be partially filled to be able to absorb low-energy photons that promote electrons from the valence band to the midgap states and from the midgap states to the conduction band, and have a finite width to minimize nonradiative recombination as much as possible (7, 9).

Atomically thin two-dimensional (2D)–based group-IV monochalcogenides, such as GeSe, are strongly anisotropic van der Waals semiconductors that are isoelectronic to black phosphorus, but with superior stability. They have emerged as promising optoelectronic materials for photovoltaic applications for several key reasons. First, GeSe exhibits low toxicity and offers a cost advantage as it is less expensive compared to materials like Ge and Sb$_2$Se$_3$. Moreover, GeSe is more than six times more earth abundant than Sb, making it a highly accessible resource (10–14). Second, the intrinsic intermolecular bonding of van der Waals interactions within the interlayer planes of 2D-based group IV monochalcogenides make them an attractive material for photovoltaic, offering a solution to the dangling bond issues that affect conventional solar absorbers. These features make them an emerging material for photovoltaic applications over conventional commercial solar cell–based materials such as Cu(In,Ga)Se$_2$ and CdTe, which require toxic or rare earth elements (15, 16). For example, GeSe exhibits attractive optoelectronic properties such as high carrier mobility, closely placed indirect and direct bandgaps, enabling tunability from 1.1 to ~1.5 eV, overlapping fairly well with the solar spectrum for a single-junction solar cell. In addition, it exhibits high absorbance near the absorption onset, allowing for the absorption of most solar radiation above the bandgap within a thin layer of 1-μm thickness (17, 18).

Layered heterostructures, formed by rationally stacking of at least two different materials and chemically functionalizing them via intercalation, offer a highly promising platform for achieving unprecedented optoelectronic device efficiency. Intercalation, which involves incorporating guest species such as ions and atoms between the layers of heterostructures, is a superior and innovative method for tuning material properties compared to traditional techniques like chemical doping or defect/strain engineering (19–25). Specifically, for atomically thin 2D-based group IV monochalcogenides,

Department of Physics, Lehigh University, Bethlehem, PA 18015, USA.
*Corresponding author. Email: che218@lehigh.edu

their vertically stacked layers host intrinsic van der Waals gap >3 Å with interlayer interactions that are mediated by weak van der Waals forces, making them particularly suitable for the intercalation technique. This process enables precise tuning of interfacial properties, including electronic structure, band alignment, and doping level, through controlled insertion or removal of guest species between the van der Waals gap of the host material. The host lattice structure remains minimally disrupted, enabling tailored control of device performance. Moreover, intercalation can enhance the stability of heterostructures, which is a critical factor for device longevity and practicality (*26*).

In this work, we have engineered intermediate band states in a 2D van der Waals quantum material composed of GeSe and SnS heterostructure (Cu$_x$GeSe/SnS) by chemically intercalating zerovalent atoms, such as Cu. The designed quantum material exhibits unique properties and potential applications in energy conversion. Our ab initio modeling revealed that the intermediate band states only emerge when many-body effects are present, regardless of the number of Cu atoms within the van der Waals gap of the 2D host materials. This finding suggests an advanced material at the Mott-Anderson limit (*27*). The primary results presented are for $x = 1$, representing the intercalation of a single Cu atom. The Cu$_x$GeSe/SnS system exhibits a many-body intermediate energy bandgap with subband gap values of ~0.78 and 1.26 eV, which is remarkably close to the optimal subband gaps (~0.71 and 1.24 eV) proposed by Luque and Martí (*2*) for efficient design of intermediate band solar cell devices. The exciton absorption spectra obtained by solving the Bethe-Salpeter equations (BSEs) (*28*) reveal high absorption in the infrared and visible regions of the electromagnetic spectrum. To evaluate the usefulness of the designed material for next-generation photovoltaic applications, we integrated it as an active layer in a solar cell device. The prototype device exhibits an average absorption of 80%, a high generation rate of photoexcited carriers, and an external quantum efficiency (EQE) that span between 110 and >190% over a broad range of solar wavelengths, including the pivotal near-infrared and visible light spectrum. We demonstrate that this high optical activity and EQE in the near-infrared and visible light range are independent of the thickness of the Cu$_x$GeSe/SnS active layer. Instead, adjusting the thickness of the Cu$_x$GeSe/SnS active layer enables tuning for enhanced optical activity and EQE in wavelengths ranging from 600 to 1200 nm.

RESULTS

To determine the stability and bonding character of the Cu intercalant with the host systems and the nature of the interfacial carriers dynamics, we modeled charge transfer and sum of the bond orders using density-derived electrostatic and chemical net atomic charges (*29–31*). We obtain a net charge transfer of $\delta \approx 1.48|e|$ to the GeSe layer and $1.21|e|$ to the SnS layer from the Cu atom, indicating *p*-type conductivity with an average doping concentration of 3%, which corresponds to approximately $10^{12}e/cm^2$. Our findings also suggest that Cu atoms do not cluster with one another but rather form ionic-like bonds with the chalcogen atoms in their vicinity (see fig. S2 in the Supplementary Materials). We can explain this scenario by considering the physical process of Cu intercalation in the van der Waals gap. As Cu atoms are introduced into the gap, the van der Waals gap contracts by ~8.05% to accommodate the guest atoms, resulting in an energetic gain. In addition, the formation of

Cu-chalcogen bonds also yields an energetic gain because the basal plane chalcogens have a negligible activation energy cost. In a typical Cu clustering process, the bonds between Cu atoms and neighboring anions gradually weaken. However, in our material system, the ionic character of the Cu-chalcogen bonds remains virtually unchanged despite the presence of Cu atoms.

To visualize the dynamics of the charge transfer, we computed the charge density difference $\delta\rho = \rho(Cu_xGeSe/SnS) - \rho(GeSe/SnS) - \rho(Cu)$, where ρ is the charge density in e/Å^3 (Fig. 1A). The blue color indicates charge depletion, which mainly occurs at the transition metal atoms (Ge and Sn) sites, while the red color indicates charge accumulation at the Cu atom site, where carriers are quasi-localized. We observed an sp^3-like hybridization between the Cu atom and the nearby chalcogen atoms. To transfer charge across the heterojunction, an energy barrier of 5.29 ± 0.05 eV and a transfer distance of $\sim 5.20 \pm 0.05$ Å must be overcome (fig. S3). This implies that electron-hole dynamics across the heterojunction are both energetically and spontaneously spatially separated, leading to the formation of interlayer excitons (*32, 33*). The spontaneous polarization effects induced by the charge transfer confine charges at the interface spatially, resulting in a substantial built-in voltage $\Delta\Phi \sim 5.19$ eV. We note that because of the distorted crystal structure of the host GeSe (SnS) material, an intrinsic $\Delta\Phi \sim 3.37$ (4.33 eV) already exists in the atomic layers (fig. S3). The proposed photovoltaic application is supported by a favorable built-in voltage and spatially confined carriers. This combination enables photogenerated carriers at the heterojunction to separate and move away from each other, reducing the likelihood of nonradiative recombination, and thus enhance carrier transport.

Figure 1B presents the many-body electronic properties for Cu$_x$GeSe/SnS ($x = 1$). Additional details are available in the Supplementary Materials. We predict a quasiparticle energy bandgap $E_g \sim 1.35$ eV for the pristine heterostructure (fig. S4A). When the heterobilayer is intercalated with Cu, intermediate band states emerge with subband gaps $E_L \sim 0.78$ and $E_H \sim 1.26$ eV (Fig. 1, B and C, and fig. S4B). The predicted subband gaps are remarkably close to the optimal values of 0.71 and 1.24 eV proposed by Luque and Martí for efficient design of next-generation photovoltaic devices (*2*). We investigated the evolution of the subband gaps as a function of Cu atoms, up to four Cu atoms intercalated within the van der Waals gap of the heterostructure. The subband gaps remained robust (see fig. S5), but the optimal values occur for one Cu atom intercalation. Our analysis of the atomic projected density of states reveals that these intermediate band states are formed by the hybridization between Cu-*s* and *p* states and the *p* states of Ge and Sn atoms (fig. S4B). Our calculations indicate that the intermediate band states are primarily driven by many-body effects. To validate this assertion, we performed a set of additional calculations with six density functional theory (DFT)–derived functionals, including the HSE06 hybrid functional (*34–39*) and found no intermediate band states in all cases (fig. S6 and table S4). Recent ultrafast terahertz experiments on GeSe and GeS bilayers showed a decrease in photoexcited carrier lifetime upon Cu intercalation, which was attributed to scattering off of quasi-localized sites formed by intermediate states, in agreement with our computational results (*40, 41*).

Inherent quantum confinement effects have a substantial impact on the electronic structure of the hybrid quantum material. It is therefore natural to investigate how quantum confinement effects influence the excitonic absorption properties of the Cu$_x$GeSe/SnS van der Waals quantum material, such as the valence electron
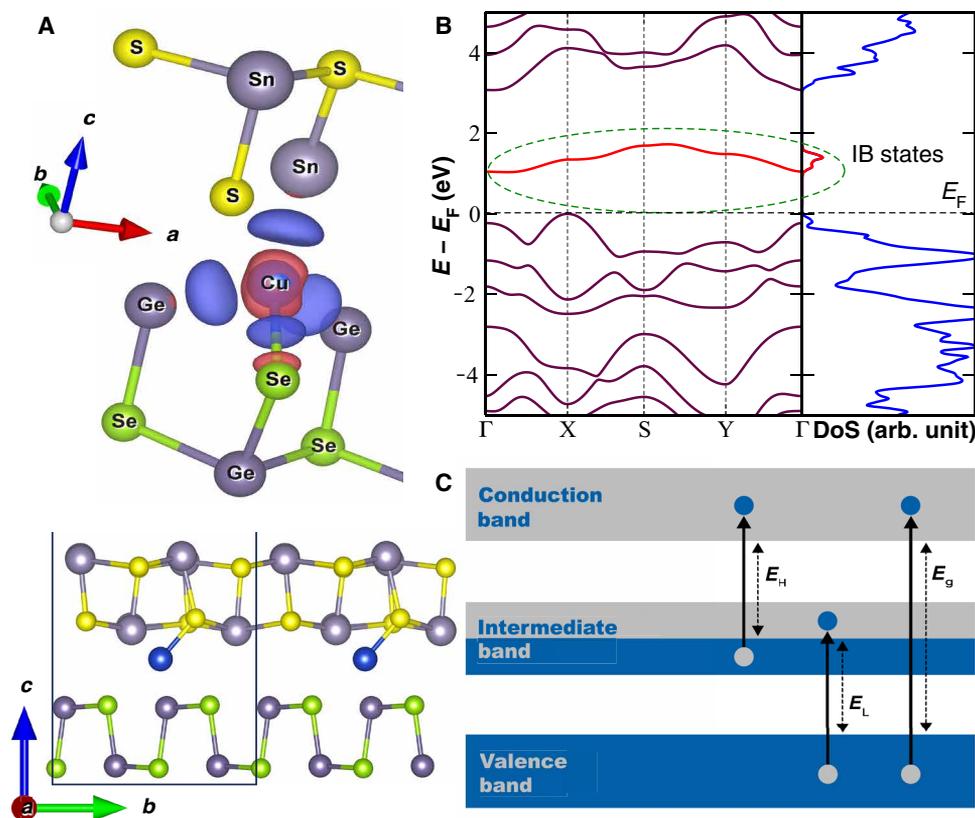
Fig. 1. Structural and electron properties of Cu$_x$GeSe/SnS. (**A**) Charge density difference in the crystal structure of Cu$_x$GeSe/SnS, illustrating positive (negative) charges depicted in blue (red), (**B**) the many-body self-consistent quasiparticle Green's function and screened Coulomb interactions electronic band structure and total density of states (DoS) depicting the intercalation-induced midgap states, and (**C**) a schematic band diagram of an intermediate band (IB) semiconductor, color-coded for the electrons (blue) and holes (gray).

energy-loss spectra (VEELS). The VEELS $L(E) = \Im[-\epsilon(E)^{-1}]$ (where $\epsilon(E)$ is the complex dynamical dielectric function), which occurs for photon energies less than ~50 eV, is a signature of collective valence state excitations, low-energy interband transitions of single electrons, possible metastable excitons, and plasmonic loss associated with the experimental single scattering distribution through $L(E)$. Figure 2 presents the VEELS for the heterostructure and the Cu-intercalated quantum system along the $\Gamma - X$ (or the zigzag) and $\Gamma - Y$ (or the armchair) directions. Additional absorption features, such as $\epsilon(E)$, are presented in fig. S7 in the Supplementary Materials. The exciton absorption spectra exhibit a unique and anisotropic photoresponse that is reminiscent of the crystal structure. In the pristine heterostructure shown in Fig. 2A, absorption onset occurs around 2.30 eV, with a plasmonic peak at 3.31 and 2.58 eV along the zigzag and armchair directions, respectively.

After intercalation, these sharp features are substantially modified into a band of absorption in the energy range of 2 to 4 eV. Cu intercalation caused a strong enhancement of absorption and substantial modification of the exciton spectra, resulting in a strong red shift and new features, especially in the near-infrared and visible light regime of the solar radiation. The EELS spectra exhibit low-energy exciton peak structure spanning from near-infrared to the ultraviolet regime. These low-energy features are due to the generation of free electron-hole pairs from the absorption of quasi-localized excitonic states below the subband E_L of the intermediate states. The plasmonic peak structure predicted in the pristine material vanished,

and new transition features emerged in the near-infrared regime. These correspond to a peak structure around 0.27 eV and a shoulder at 0.49 eV along the x and y directions, respectively. We predict interband transitions from the valence to the intermediate band states at 0.97 and ~1.01 eV along the x and y directions (Fig. 2B). The observed substantial increase in absorption could be advantageous for next-generation solar cell applications, benefiting from large absorption in the 0.27- to 4.50-eV range, which dominates the solar irradiance spectrum in the visible and near-infrared regions.

Motivated by the unique and high absorption in the regime of rich solar irradiance observed in the designed Cu-intercalated quantum material, which are promising for next-generation photovoltaic applications, we designed and modeled a thin-film solar cell with the Cu$_x$GeSe/SnS quantum material as the active layer. The choice of components in solar devices greatly affects device performance, characterized by the figure of merit such as the EQE. One major challenge in designing solar cell devices is the choice of the metal electrode at the semiconductor-metal interface. These interfaces are often characterized by complex interfacial reconstruction and a high Schottky barrier height Φ_{SBH}, which reduces carrier transfer efficiency. While Au has been extensively used as a back electrode in solar cell devices, we modeled the X-Au interface, where X is Cu$_x$GeSe/SnS active layer, to determine its suitability in our case. Our model shows a relatively low tunneling barrier of $\Delta V \sim 0.21$ eV and a low quasi-ohmic contact with $\Phi_{SBH} \sim 0.07$. The favorable ΔV and Φ_{SBH} support high carrier injection efficiency. The predicted Φ_{SBH} agrees
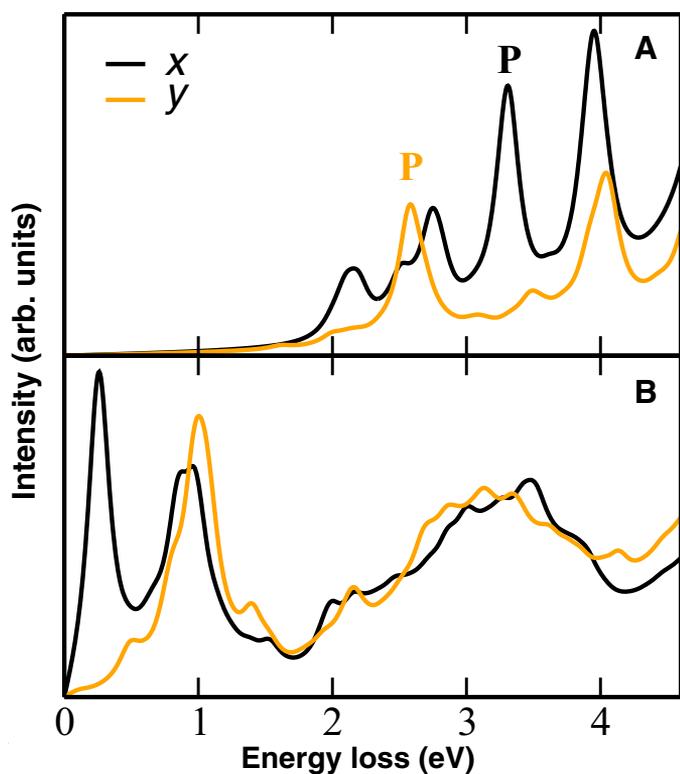
Fig. 2. Low-energy exciton loss spectra L of CuxGeSe/SnS. *L* obtained with the GW-BSE for (**A**) GeSe/SnS and (**B**) CuxGeSe/SnS along the $\Gamma - X$ (*x*-direction) and $\Gamma - Y$ (*y*-direction) directions. "P" denotes plasmon peak.

with previous studies that showed Au to be a good electrode in GeSe thin-film solar cells (*10*, *42*) and is much lower than those of other semiconductor-Au systems (*43*).

Using the exciton spectra from our many-body calculations, we characterized the active layer of the solar cell device and simulated it under solar irradiation in air mass 1.5G. (*44*) We used transparent conducting films of indium tin oxide (ITO) as the front electrode and Au thin films as the back electrode, while ZnO served as the window layer. The resulting solar cell device has the structure: ITO/ZnO/*X*/Au (Fig. 3A). Central to the device modeling is the complex refractive index, defined as $\tilde{n} = n + ik$; it is directly related to the exciton complex dielectric function from our many-body BSE calculations, where *n* denotes the refractive index and *k* represents the extinction coefficient. In conventional bulk materials, $\tilde{n}$ is an intrinsic and invariant attribute of a material, being primarily influenced by its composition and light-matter interactions, rather than by geometric attributes like thickness or dimension (*45*). However, in 2D-based materials, the electronic and optical properties are markedly enhanced and deeply sensitive to the number of layers. This paradigm of size-dependent physical properties (in contrast to the invariant behavior of bulk materials) is now accepted as an intrinsic property. The fundamental thickness of the CuxGeSe/SnS active layer approximated with the unit cell dimension along the *z* axis is ~2 nm (fig. S1). We modeled and characterized a solar cell device incorporating the fundamental thickness of the CuxGeSe/SnS active layer. To determine the efficiency of the solar cell device, we computed the external quantum efficiency $EQE(\%) = 1240 \times \frac{J_{sc}}{\lambda I_0}$, where

I_0 (in units of W/m^2) is the intensity of the incident solar radiation (*46*). The EQE of photovoltaic devices is a critical performance metric that quantifies the conversion efficiency of incident solar radiation into electrical energy. Notably, in intermediate band materials, EQE can exceed 100% because of a two-photon process emanating from MEG processes. The solar cell device designed with the fundamental thickness exhibited high EQE that span between 110 and >190 % within the infrared and visible regions of the electromagnetic spectrum (Fig. 3). Notably, this wavelength range matches the high absorption found in the exciton absorption spectra.

To guide experimental synthesis using the CuxGeSe/SnS quantum material as an active layer in solar cell devices, we explored how device efficiency evolves when altering the active-layer thickness from the atomic scale to the nanoscale. We examined the light-matter interactions in the solar cell device by varying the CuxGeSe/SnS active-layer thickness from the fundamental lower limit of ~2 nm adopting thickness-independent complex refractive index. While intrinsic quantum confinement in CuxGeSe/SnS quantum material might induce variations, within the scale of our numerical modeling, $\tilde{n}$ can be approximated as thickness independent. Recent experiments on 2D transition metal dichalcogenides show that, while $\tilde{n}$ does change with thickness, this change remains below 5% for up to three layers (*47*). Furthermore, typical thin films exhibit minimal refractive index dependence on thickness, specifically between 200 and 800 nm, deviating by roughly 0.10 (*48*).

In our design, atomically thin GeSe and SnS are vertically stacked, facilitating the easy integration of the hybrid structures through van der Waals interactions. The thickness-dependent modeling of the solar device efficiency indicate that the high EQE observed in the device using the fundamental active-layer thickness remains consistent across the 400- to ~560-nm wavelength range, encompassing both infrared and visible domains. However, obtaining a substantial EQE between 600 and ~1200 nm demands a thicker active layer, probably due to the spatial delay in charge carrier generation as wavelength increases (fig. S8). This highlights the need for tailoring active-layer thickness to optimize peak efficiency zones in photovoltaic systems. Designing solar cell devices often entails determining the optimal active-layer thickness, maximizing both device efficiency and the total short-circuit current J_{sc}, the highest current extractable from a solar cell under ideal conditions. By examining the evolution of the prototype solar device and modeling J_{sc} dependence on the thickness of the active layer (fig. S9), we systematically determine the optimal thickness of the CuxGeSe/SnS active layer to be around 250 nm with an optimal J_{sc} of ~43.54 mA/cm^2. Using these parameters, we assessed the total wavelength-dependent reflectivity and transmissivity for each solar cell component and the photogenerated carrier generation rate (Fig. 3, B and C). The solar radiation transmission through the device is minimal, with total reflectivity fluctuating between 0 and 20% across the entire wavelength range. The active layer displays notable absorption, peaking at >90% across a broad wavelength range and maintaining over 65% up to λ ~ 1250 nm, where it then gradually decreases (Fig. 3B). The photogenerated carrier generation rate profile (Fig. 3C) shows that most carriers form within the active layer, notably in the 400- to 650-nm wavelength range. As depicted in Fig. 3D, the calculated EQE fluctuates between 110 and >190% at pivotal wavelengths.

The high EQE zones are notably aligned with the critical solar radiation spectra of near-infrared and visible light. This alignment, alongside large absorption and the emergence of intermediate band
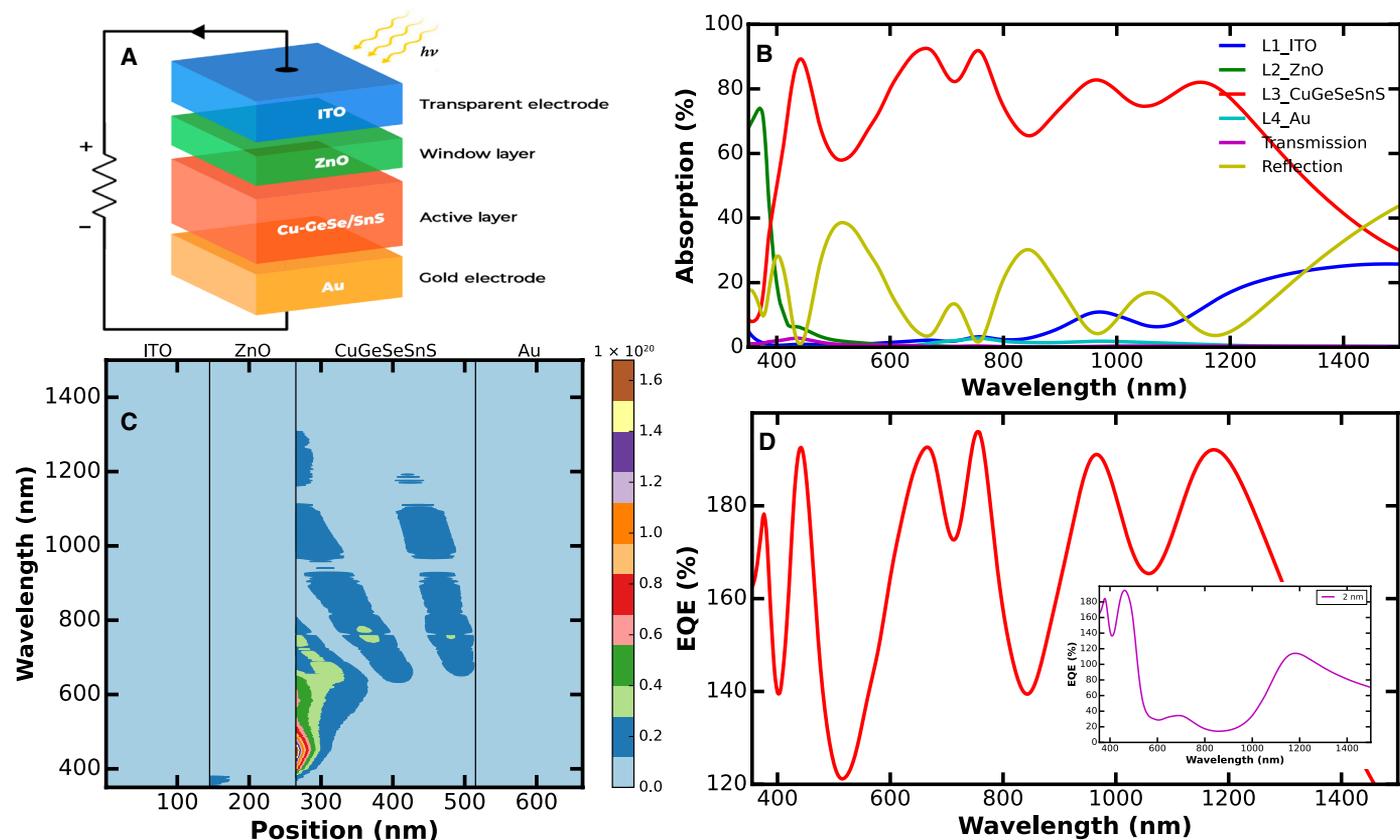
Fig. 3. Design architecture and the device characteristics of solar cell with Cu$_x$GeSe/SnS as active layer. (**A**) Schematic of the thin-film solar cell with Cu$_x$GeSe/SnS as the active layer, (**B**) the layer-dependent excitonic absorption spectra consisting of the total reflection and total transmission, (**C**) the generation rate of photoexcited excitons as a function of the solar wavelength and position in the device, and (**D**) the profile of the dependence of the EQE on the wavelength of the solar radiation for solar device incorporating the optimal active-layer thickness. The inset in (D) shows the EQE of a solar cell with the fundamental active-layer thickness. Note the consistent nature of the EQE within the crucial solar wavelength range, spanning the near-infrared and visible spectrum.

states, is further supported by recent experimental results that reported the emergence of intermediate band states in Cu-intercalated, Ge-based group IV materials (*40, 41*). Ultrafast measurements revealed distinct photoconductivity responses in both pristine and Cu-intercalated Ge-based nanoribbons following 800-nm pulse excitation. While pristine GeS nanoribbons exhibit a photoluminescence decay time ranging between 30 and 60 ps, Cu-intercalated samples show a notably rapid decay of only 5 to 9 ps. Moreover, the observation of longer lifetimes at elevated excitation fluences suggests trap site saturation. These emerging characteristics, particularly the rapid response and enhanced efficiency in Cu-intercalated samples, strongly indicate the potential of Cu-intercalated GeSe/SnS as a quantum material for use in advanced photovoltaic applications, offering an avenues for efficiency improvements in solar energy conversion. This synergy between predicted performance and experimental findings underscores the potential of these materials in solar energy applications.

DISCUSSION

We investigated the promising capabilities of a distinctive quantum material formed by the intercalation of zerovalent Cu atoms into the van der Waals gap within the atomically thin GeSe/SnS heterostructure. This material was investigated for its potential application as the active layer in energy-efficient photovoltaic devices.

Our computational studies revealed that this material exhibits intermediate band states, which are predominantly influenced by many-body effects. These intermediate states facilitate enhanced absorption capabilities across both the near-infrared and visible light spectra. This characteristic is critically important for the efficient capture and conversion of solar radiation, a key parameter in photovoltaic technology. Notably, the material demonstrated an ability to potentially exceed the conventional limits of solar cell efficiency. In our simulations, a solar cell incorporating our designed quantum material as the active layer showed the potential to achieve a quantum efficiency as high as 190% across a broad range of solar wavelengths. This finding is particularly noteworthy as it suggests the possibility of surpassing the Shockley-Queisser limit, a theoretical maximum efficiency for a single-junction solar cell under standard test conditions. The GeSe/SnS-based quantum material, therefore, stands as a highly promising candidate for the development of next-generation, high-efficient solar cells, which will play a crucial role in addressing global energy needs. While the practical integration of the designed quantum material into existing photovoltaic systems remains an area for further refinement, it is important to acknowledge that the experimental process for creating such materials is already well-established. The intercalation of zerovalent elements into the van der Waals gaps of atomically thin layered materials at the nanoscale, leveraging advanced technologies, is a well-established and reliable technique.

This method has been refined through extensive research, proving its effectiveness in producing innovative quantum materials.

MATERIALS AND METHODS
Quantum computational methods

The optoelectronic properties of Cu_xGeSe/SnS quantum materials were obtained using ab initio many-body, self-consistent quasiparticle Green's function plus screened Coulomb interactions (scQPGW) approach for the many-body electronic ground state and the BSE for the exciton optical transport spectra (*49–56*) as implemented in VASP (*57*). All computations incorporated van der Waals interactions via the DFT-D3 parameterization (*58, 59*), and projector augmented wave potentials that included an accurate account of electron-electron and electron-hole interactions, and an optimized set of potentials to properly account for excited state properties. We performed series of benchmarking calculations to determine the optimal set of input parameters that converges the quasiparticle bandgap and states to at least within 10 meV (*60, 61*) (see details in the Supplementary Materials). On the basis of our detailed benchmarking calculations, we adopted a $3 \times 3 \times 1$ Γ-centered grid to represent the reciprocal space and an energy cutoff of 500 eV (160 eV) for the DFT (scQPGW). Our many-body calculations used 120 additional empty bands and 20 virtual and occupied bands for the scQPGW calculations, and the solutions of the BSE, respectively. Hybrid Cu_x-GeSe/SnS quantum materials were designed by chemically intercalating zerovalent Cu atoms into the intrinsic van der Waals gap between a $2 \times 2 \times 1$ supercell of atomically thin GeSe and SnS structures, both of which exhibit orthorhombic crystal symmetry (space group $Pmn2_1$) (*15, 16, 62, 63*) with <2% lattice mismatch. Using DFT, the hybrid quantum materials were first optimized until the energy (charge) was converged to within 10^{-3} (10^{-7} eV) and residual stresses (forces) dropped to approximately 10^{-1} GPa (10^{-3} eVÅ^{-1}) using the Perdew-Burke-Ernzerhof exchange-correlation functional (*64*). The size of the van der Waals gap decreased from ~3.23 to 2.97 Å after Cu intercalation and structural relaxation (Fig. 1A and fig. S1). The synthesis feasibility of the designed quantum materials was established through energetic, structural, and mechanical stability calculations and analyses using the ElasTool computational toolkit (*65*) (see table S1).

Device modeling

A solar cell device using the designed Cu_xGeSe/SnS as the active layer was designed and characterized to determine the efficiency. The essential parameter in the device calculations is the complex refractive index. For the active layer, this is provided by the exciton absorption spectra from the scQPGW + BSE advanced calculations, ensuring that many-body effects are accurately incorporated into the solar cell device design. The performance of the device was methodically investigated using the numerically exact transfer matrix method, adopting the approach proposed and successfully used by Pettersson *et al.* (*46*) in their seminal work. The transfer matrix method code used for the device modeling is provided in our GitHub website (*66*) and from 10.5281/zenodo.10780496.

Supplementary Materials

This PDF file includes:
Supplementary Text
Figs. S1 to S9
Tables S1 to S5
References

REFERENCES AND NOTES

1. W. Shockley, H. J. Queisser, Detailed balance limit of efficiency of *p-n* junction solar cells. *J. Appl. Phys.* **32**, 510–519 (1961).
2. A. Luque, A. Martí, Increasing the efficiency of ideal solar cells by photon induced transitions at intermediate levels. *Phys. Rev. Lett.* **78**, 5014–5017 (1997).
3. C. Smith, D. Binks, Multiple exciton generation in colloidal nanocrystals. *Nanomaterials* **4**, 19–45 (2013).
4. L. A. Padilha, J. T. Stewart, R. L. Sandberg, W. K. Bae, W.-K. Koh, J. M. Pietryga, V. I. Klimov, Carrier multiplication in semiconductor nanocrystals: Influence of size, shape, and composition. *Acc. Chem. Res.* **46**, 1261–1269 (2013).
5. A. Luque, A. Martı, C. Stanley, N. López, L. Cuadra, D. Zhou, J. Pearson, A. McKee, General equivalent circuit for intermediate band devices: Potentials, currents and electroluminescence. *J. Appl. Phys.* **96**, 903–909 (2004).
6. E. Antolin, A. Martí, P. G. Linares, I. Ramiro, E. Hernández, C. Farmer, C. Stanley, A. Luque, Advances in quantum dot intermediate band solar cells, in *2010 35th IEEE Photovoltaic Specialists Conference* (IEEE, 2010), pp. 000065–000070.
7. A. Luque, A. Martí, The intermediate band solar cell: Progress toward the realization of an attractive concept. *Adv. Mater.* **22**, 160–174 (2010).
8. M.-J. Sher, E. Mazur, Intermediate band conduction in femtosecond-laser hyperdoped silicon. *Appl. Phys. Lett.* **105**, 032103 (2014).
9. A. Luque, A. Martí, C. Stanley, Understanding intermediate-band solar cells. *Nat. Photonics* **6**, 146–152 (2012).
10. D.-J. Xue, J. Tan, J.-S. Hu, W. Hu, Y.-G. Guo, L.-J. Wan, Anisotropic photoresponse properties of single micrometer-sized gese nanosheet. *Adv. Mater.* **24**, 4528–4533 (2012).
11. D. D. I. Vaughn, R. J. Patel, M. A. Hickner, R. E. Schaak, Single-crystal colloidal nanosheets of GeS and GeSe. *J. Am. Chem. Soc.* **132**, 15170–15172 (2010).
12. R. Fei, W. Li, J. Li, L. Yang, Giant piezoelectricity of monolayer group IV monochalcogenides: SnSe, SnS, GeSe, and GeS. *Appl. Phys. Lett.* **107**, 173104 (2015).
13. E. Akhoundi, M. Faghihnasiri, S. Memarzadeh, A. H. Firouzian, Mechanical and strain-tunable electronic properties of the sns monolayer. *J. Phys. Chem. Solid* **126**, 43–49 (2019).
14. X. Song, W. Zhou, X. Liu, Y. Gu, S. Zhang, Layer-controlled band alignment, work function and optical properties of few-layer gese. *Physica B Condens. Matter* **519**, 90–94 (2017).
15. Y. Mao, C. Xu, J. Yuan, H. Zhao, A two-dimensional GeSe/SnSe heterostructure for high performance thin-film solar cells. *J. Mater. Chem. A* **7**, 11265–11271 (2019).
16. N. Maity, P. Srivastava, H. Mishra, R. Shinde, A. K. Singh, Anisotropic interlayer exciton in gese/sns van der waals heterostructure. *J. Phys. Chem. Lett.* **12**, 1765–1771 (2021).
17. L. Xu, M. Yang, S. J. Wang, Y. P. Feng, Electronic and optical properties of the monolayer group-IV monochalcogenides *MX* (*M* = Ge, Sn; *X* = S, Se, Te). *Phys. Rev. B* **95**, 235434 (2017).
18. L. C. Gomes, P. E. Trevisanutto, A. Carvalho, A. S. Rodin, A. H. Castro Neto, Strongly bound Mott-Wannier excitons in GeS and GeSe monolayers. *Phys. Rev. B* **94**, 155428 (2016).
19. G. Doll, J. Speck, G. Dresselhaus, M. Dresselhaus, K. Nakamura, S.-I. Tanuma, Intercalation of hexagonal boron nitride with potassium. *J. Appl. Phys.* **66**, 2554–2558 (1989).
20. X. Zhao, P. Song, C. Wang, A. C. Riis-Jensen, W. Fu, Y. Deng, D. Wan, L. Kang, S. Ning, J. Dan, T. Venkatesan, Z. Liu, W. Zhou, K. S. Thygesen, X. Luo, S. J. Pennycook, K. P. Loh, Engineering covalently bonded 2D layered materials by self-intercalation. *Nature* **581**, 171–177 (2020).
21. C. Stern, A. Twitto, R. Z. Snitkoff, Y. Fleger, S. Saha, L. Boddapati, A. Jain, M. Wang, K. J. Koski, F. L. Deepak, A. Ramasubramaniam, D. Naveh, Enhancing light–matter interactions in MoS$_2$ by copper intercalation. *Adv. Mater.* **33**, e2008779 (2021).
22. Y. Gong, H. Yuan, C.-L. Wu, P. Tang, S.-Z. Yang, A. Yang, G. Li, B. Liu, J. van de Groep, M. L. Brongersma, M. F. Chisholm, S. C. Zhang, W. Zhou, Y. Cui, Spatially controlled doping of two-dimensional SnS$_2$ through intercalation for electronics. *Nat. Nanotechnol.* **13**, 294–299 (2018).
23. J. Yao, K. J. Koski, W. Luo, J. J. Cha, L. Hu, D. Kong, V. K. Narasimhan, K. Huo, Y. Cui, Optical transmission enhancement through chemically tuned two-dimensional bismuth chalcogenide nanoplates. *Nat. Commun.* **5**, 5670 (2014).
24. I. Samaras, S. Saikh, C. Julien, M. Balkanski, Lithium insertion in layered materials as battery cathodes. *Mater. Sci. Eng. B* **3**, 209–214 (1989).
25. X.-C. Liu, S. Zhao, X. Sun, L. Deng, X. Zou, Y. Hu, Y.-X. Wang, C.-W. Chu, J. Li, J. Wu, F. S. Ke, P. M. Ajayan, Spontaneous self-intercalation of copper atoms into transition metal dichalcogenides. *Sci. Adv.* **6**, eaay4092 (2020).
26. G. Li, L. Zhang, W. Xu, J. Pan, S. Song, Y. Zhang, H. Zhou, Y. Wang, L. Bao, Y.-Y. Zhang, S. du, M. Ouyang, S. T. Pantelides, H. J. Gao, Stable silicene in graphene/silicene Van der Waals heterostructures. *Adv. Mater.* **30**, e1804650 (2018).
27. D. Belitz, T. Kirkpatrick, The Anderson-Mott transition. *Rev. Mod. Phys.* **66**, 261–380 (1994).
28. E. E. Salpeter, H. A. Bethe, A relativistic equation for bound-state problems. *Phys. Rev.* **84**, 1232–1242 (1951).
29. T. A. Manz, N. G. Limas, Introducing DDEC6 atomic population analysis: Part 1. Charge partitioning theory and methodology. *RSC Adv.* **6**, 47771–47801 (2016).
30. N. G. Limas, T. A. Manz, Introducing DDEC6 atomic population analysis: Part 2. Computed results for a wide range of periodic and nonperiodic materials. *RSC Adv.* **6**, 45727–45747 (2016).

31. T. A. Manz, Introducing DDEC6 atomic population analysis: Part 3. Comprehensive method to compute bond orders. *RSC Adv.* **7**, 45552–45581 (2017).

32. P. Rivera, H. Yu, K. L. Seyler, N. P. Wilson, W. Yao, X. Xu, Interlayer valley excitons in heterobilayers of transition metal dichalcogenides. *Nat. Nanotechnol.* **13**, 1004–1015 (2018).

33. Y. Jiang, S. Chen, W. Zheng, B. Zheng, A. Pan, Interlayer exciton formation, relaxation, and transport in TMD van der Waals heterostructures. *Light Sci. Appl.* **10**, 72 (2021).

34. A. V. Krukau, O. A. Vydrov, A. F. Izmaylov, G. E. Scuseria, Influence of the exchange screening parameter on the performance of screened hybrid functionals. *J. Chem. Phys.* **125**, 224106 (2006).

35. J. Sun, A. Ruzsinszky, J. P. Perdew, Strongly constrained and appropriately normed semilocal density functional. *Phys. Rev. Lett.* **115**, 036402 (2015).

36. A. P. Bartók, J. R. Yates, Regularized SCAN functional. *J. Chem. Phys.* **150**, 161101 (2019).

37. J. W. Furness, A. D. Kaplan, J. Ning, J. P. Perdew, J. Sun, Accurate and numerically efficient r^{2}SCAN meta-generalized gradient approximation. *J. Phys. Chem. Lett.* **11**, 8208–8215 (2020).

38. J. Sun, M. Marsman, G. I. Csonka, A. Ruzsinszky, P. Hao, Y.-S. Kim, G. Kresse, J. P. Perdew, Self-consistent meta-generalized gradient approximation within the projector-augmented-wave method. *Phys. Rev. B* **84**, 035117 (2011).

39. Y. Zhao, D. G. Truhlar, A new local density functional for main-group thermochemistry, transition metal bonding, thermochemical kinetics, and noncovalent interactions. *J. Chem. Phys.* **125**, 194101 (2006).

40. L. V. Titova, K. Kushnir, S. Khanmohammadi, C. Tran, E. Colin-Ulloa, C. Ekuma, K. Koski, *Terahertz Emitters, Receivers, and Applications XIV* (SPIE, 2023).

41. S. Khanmohammadi, K. Kushnir Friedman, E. Chen, S. Kastuar, C. Ekuma, K. Koski, L. Titova, Tailoring ultrafast near band gap photoconductive response in GeS by zero-valent Cu intercalation. *ACS Appl. Mater. Interfaces*, (2024). in press.

42. D.-J. Xue, S.-C. Liu, C.-M. Dai, S. Chen, C. He, L. Zhao, J.-S. Hu, L.-J. Wan, Gese thin-film solar cells fabricated by self-regulated rapid thermal sublimation. *J. Am. Chem. Soc.* **139**, 958–965 (2017).

43. Y. Pan, Y. Dan, Y. Wang, M. Ye, H. Zhang, R. Quhe, X. Zhang, J. Li, W. Guo, L. Yang, J. Lu, Schottky barriers in bilayer phosphorene transistors. *ACS Appl. Mater. Interfaces* **9**, 12694–12705 (2017).

44. Best research-cell efficiency chart https://www.nrel.gov/pv/cell-efficiency.html.

45. M. Born, E. Wolf, *Principles of Optics: Electromagnetic Theory of Propagation, Interference and Diffraction of Light* (Cambridge Univ. Press, 1999).

46. L. A. Pettersson, L. S. Roman, O. Inganäs, Modeling photocurrent action spectra of photovoltaic devices based on organic thin films. *J. Appl. Phys.* **86**, 487–496 (1999).

47. C. Hsu, R. Frisenda, R. Schmidt, A. Arora, S. M. de Vasconcellos, R. Bratschitsch, H. S. J. van der Zant, A. Castellanos-Gomez, Thickness-dependent refractive index of 1L, 2L, and 3L MoS$_2$, MoSe$_2$, WS$_2$, and WSe$_2$. *Adv. Opt. Mater.* **7**, 1900239 (2019).

48. G. Georgescu, A. Petris, Analysis of thickness influence on refractive index and absorption coefficient of zinc selenide thin films. *Opt. Express* **27**, 34803–34823 (2019).

49. M. Shishkin, M. Marsman, G. Kresse, Accurate quasiparticle spectra from self-consistent gw calculations with vertex corrections. *Phys. Rev. Lett.* **99**, 246403 (2007).

50. S. Albrecht, L. Reining, R. Del Sole, G. Onida, Ab initio calculation of excitonic effects in the optical spectra of semiconductors. *Phys. Rev. Lett.* **80**, 4510–4513 (1998).

51. M. Rohlfing, S. G. Louie, Electron-hole excitations in semiconductors and insulators. *Phys. Rev. Lett.* **81**, 2312–2315 (1998).

52. M. Shishkin, G. Kresse, Self-consistent *GW* calculations for semiconductors and insulators. *Phys. Rev. B* **75**, 235102 (2007).

53. F. Gross, *Relativistic Quantum Mechanics and Field Theory* (a Wiley-Interscience publication, Wiley, 1999).

54. A. Fetter, J. Walecka, *Quantum Theory of Many-Particle Systems* (Dover Books on Physics, Dover Publishers, 1971).

55. S. V. Faleev, M. van Schilfgaarde, T. Kotani, All-electron self-consistent *GW* approximation: Application to Si, MnO, and NiO. *Phys. Rev. Lett.* **93**, 126406 (2004).

56. L. Hedin, New method for calculating the one-particle green's function with application to the electron-gas problem. *Phys. Rev.* **139**, A796–A823 (1965).

57. G. Kresse, J. Furthmüller, Efficiency of ab-initio total energy calculations for metals and semiconductors using a plane-wave basis set. *Comput. Mater. Sci.* **6**, 15–50 (1996).

58. S. Grimme, J. Antony, S. Ehrlich, H. Krieg, A consistent and accurate ab initio parametrization of density functional dispersion correction (DFT-D) for the 94 elements H-Pu. *J. Chem. Phys.* **132**, 154104 (2010).

59. S. Grimme, S. Ehrlich, L. Goerigk, Effect of the damping function in dispersion corrected density functional theory. *J. Comput. Chem.* **32**, 1456–1465 (2011).

60. D. Y. Qiu, F. H. da Jornada, S. G. Louie, Optical spectrum of mos$_2$: Many-body effects and diversity of exciton states. *Phys. Rev. Lett.* **111**, 216805 (2013).

61. C. Ekuma, Optical absorption in monolayer SnO2. *Phys. Rev. B* **99**, 075421 (2019).

62. J.-D. Zheng, Y.-F. Zhao, Z.-Q. Bao, Y.-H. Shen, Z. Guan, N. Zhong, F.-Y. Yue, P.-H. Xiang, C.-G. Duan, Flexoelectric effect induced p–n homojunction in monolayer GeSe. *2D Mater.* **9**, 035005 (2022).

63. A. Jain, S. P. Ong, G. Hautier, W. Chen, W. D. Richards, S. Dacek, S. Cholia, D. Gunter, D. Skinner, G. Ceder, K. A. Persson, Commentary: The materials project: A materials genome approach to accelerating materials innovation. *APL Mater.* **1**, 011002 (2013).

64. J. P. Perdew, K. Burke, M. Ernzerhof, Generalized gradient approximation made simple. *Phys. Rev. Lett.* **77**, 3865–3868 (1996).

65. Z.-L. Liu, C. Ekuma, W.-Q. Li, J.-Q. Yang, X.-J. Li, ELASTOOL: An automated toolkit for elastic constants calculation. *Comput. Phys. Commun.* **270**, 108180 (2022).

66. Optical modeling with numerically exact transfer matrix method, *GitHub Repository for Prototype Device Modeling* (2023); https://github.com/gmp007/Optical-Modeling-of-Next-Gen-IB-Photovoltaics [accessed 21 August 2023].

ScienceAdvances

Chemically tuned intermediate band states in atomically thin Cu$_x$GeSe/SnS quantum material for photovoltaic applications

Srihari M. Kastuar and Chinedu E. Ekuma

View the article online
https://www.science.org/doi/10.1126/sciadv.adl6752
Permissions
https://www.science.org/help/reprints-and-permissions

Use of this article is subject to the Terms of service